Study of $B \to J/\psi\omega K$ at Belle

Rajesh Kumar Maiti

A dissertation submitted for the partial fulfillment of MS degree in Science

Indian Institute of Science Education and Research Mohali

April 2019

Certificate of Examination

This is to certify that the dissertation titled "Study of $B \to J/\psi\omega K$ at Belle" submitted by Mr. Rajesh Kumar Maiti (Reg. No. MP16006) for the partial fulfillment of MS degree programme of the Institute, has been examined by the thesis committee duly appointed by the Institute. The committee finds the work done by the candidate satisfactory and recommends that the report be accepted.

Dr. Satyajit Jena Dr. Harvinder Kaur Jassal Dr. Vishal Bhardwaj

(Supervisor)

Dated: April 24, 2019

Declaration

The work presented in this dissertation has been carried out by me under the guidance of Dr. Vishal Bhardwaj at the Indian Institute of Science Education and Research Mohali.

This work has not been submitted in part or in full for a degree, a diploma, or a fellowship to any other university or institute. Whenever contributions of others are involved, every effort is made to indicate this clearly, with due acknowledgement of collaborative research and discussions. This thesis is a bonafide record of original work done by me and all sources listed within have been detailed in the bibliography.

Rajesh Kumar Maiti

(Candidate)

Dated: April 24, 2019

In my capacity as the supervisor of the candidate's project work, I certify that the above statements by the candidate are true to the best of my knowledge.

Dr. Vishal Bhardwaj

(Supervisor)

Acknowledgement

First and foremost, I would like to express my deepest gratitude and sincerest thanks to my thesis supervisor Dr. Vishal Bhardwaj for his invaluable guidance, unfailing encouragement, taking pains in clearing many things and for his full co-operation. I would also like to thank him for allowing me to work in this beautiful field of "Experimental Particle Physics". Also, I would like to thank my thesis committee members Dr. Satyajit Jena and Dr. Harvinder Kaur Jassal for their valuable suggestions and criticism of my work.

I want to thank all my friends for supporting and helping me during the entire period of the project, especially Sourav Patra and Renu Garg for assisting me with discussions.

I want to express my gratitude towards my parents for moral support and encouragement.

I sincerely thank Belle Collaboration for providing me necessary computing tools and resources.

Finally, I acknowledge IISER Mohali for providing me best Infrastructures and environment for carrying out this project. I am also thankful to the "Ministry of Human Resource Development," Govt. of India for supporting me with institute fellowship during the past three years.

List of Figures

List of Tables

Notation

B	B meson
e^-	Electron
e^+	Positron
μ^+	Muon
μ^-	Anti-muon
ν_e	Electron neutrino
$\bar{\nu_e}$	Electron anti-neutrino
ν_μ	Muon neutrino
$\bar{\nu_\mu}$	Muon anti-neutrino
J/ψ	ψ meson
γ	Photon
ω	ω meson
$\Upsilon(nS)$	$\Upsilon(nS)$ meson
l^+l^-	Leptons
K	K meson
π	π meson
D^0	D^0 meson
E_{beam}	Beam energy
η	η meson
$M_{J/\psi\omega}$	Invariant mass of X
M_{bc}	Beam constrained mass
$\mathcal{B}$	Branching fraction
ϵ	Efficiency
1DUML	One dimensional unbinned maximum likelihood
MC	Monte Carlo
CM	Centre of mass

Contents

Abstract

Motive of this thesis is to search for $B \to XK$ decay mode, where X may be $X(3872)$ and $X(3915)$ and goes to $J/\psi\omega$, using the data sample of 772×10^6 $B\bar{B}$ pair. We performed signal Monte Carlo (MC) study for $B \to J/\psi\omega$ K decay mode and estimated the reconstruction efficiency for $B \to X(3872)$ K to be is about 9±0.1% and for $B \to X(3915)$ K is about 8.6±0.1%. Based on $B \to J/\psi X$ Inclusive MC study we expect 51±3 and 209 ±12 events for $B \to X(3872)K$ and $B \to X(3915)K$ decay mode and the corresponding branching fraction is 7.02±0.4(stat)$\times 10^{-6}$ and 3.02±0.2(stat) $\times 10^{-5}$, respectively. The used data is collected by belle detector at KEK-B asymmetric e^+e^- collider.

Chapter 1

Introduction

1.1 Mesons

Mesons are the subatomic particles composed of one quark and one antiquark. They are part of the hadrons (particle made of quarks). The other members of the hadron family are the baryons, composed of three quarks. The difference between mesons and baryons is that mesons are bosons (integer spin) while baryons are fermions (half-integer spin). Mesons are explained here as they are relevant to this thesis work. Mesons participate in both weak and strong interactions. Mesons with electric charge can also participate in the EM interaction. The classification of meson done according to their quark content, total angular momentum, parity, and various other properties such as C -parity. Mesons are less massive than most of the baryons and easily produced in experiments.

Spin represents the intrinsic angular momentum of a particle. Two quarks can have their spins aligned, and the spin vectors add to make a vector of length S =1 and three spin projections (S_z= +1, S_z=0, S_z=-1) called the spin-1 triplet. If two quarks have unaligned spins, the spin vectors add to make a vector of length S =0, and spin projection (S_z=0) called spin-0 singlet. Mesons can form triplet or singlet spin states.

1.2 $\Upsilon(4S)$ Meson

The Υ mesons are the bound state of the $b\bar{b}$. Experimental study of B physics began in 1977 when the CFS (Columbia-Fermilab-Stony Brook) Collaboration at Fermilab observed a narrow resonance at an energy of about 9.5 GeV in the reaction $p + \text{nucleus} \rightarrow \mu^+\mu^- + \text{X}$, resonance named as $\Upsilon(1S)$. Later on the Υ, mesons were confirmed by experiments at CESR and DORIS. The masses and widths of the resonances have listed in Table 1.1. The width of $\Upsilon(4S)$ resonance is significantly larger than the width of the three lighter resonances ($\Upsilon(1S)$, $\Upsilon(2S)$ and $\Upsilon(3S)$). The OZI (Okubo-Zweig-Iizuka) suppression of hadronic decays is responsible for the narrow width of the $\Upsilon(1S)$, $\Upsilon(2S)$ and $\Upsilon(3S)$ states.

The mass of $\Upsilon(4S)$ meson is just above the threshold of $B\bar{B}$ production. Although

Table 1.1: Masses and widths of Υ mesons.

Meson	Mass (MeV/c^2)	Total width (MeV)
$\Upsilon(1S)$	9460.30±0.26	0.05402±0.00125
$\Upsilon(2S)$	10023.26±0.31	0.03198±0.00263
$\Upsilon(3S)$	10355.2±0.5	0.02032±0.00185
$\Upsilon(4S)$	10579.4±1.2	20.5±2.5
$\Upsilon(5S)$	10876±11	55±28
$\Upsilon(6S)$	11019±8	79±16

KEKB machine operates at the $\Upsilon(4S)$ resonance to produce a large number of $B\bar{B}$ pairs, it also produces three times more $q\bar{q}$ events that contribute as background to the B physics. KEKB accelerator operates at 60 MeV below the $\Upsilon(4S)$ resonance to study the $q\bar{q}$ events background contribution.

1.3 Charmonium

Bound system of a quark and its own antiquark (such as $c\bar{c}$, $b\bar{b}$) is known as quarkonium. Bound system of $c\bar{c}$ known as charmonium. The charmonium family has a net charm of zero. As charmonium is made from fermion (spin 1/2); the total spin $S = 0$ or 1. The charge conjugation C-parity and P- parity of charmonium defined as

$$C = (-1)^{L+S} \tag{1.1}$$

$$P = (-1)^{L+1} \tag{1.2}$$

The bound state of $c\bar{c}$ is considered to be a non-relativistic system with a spin-independent central potential defined as,

$$V(r) = -\frac{4\alpha_s}{3r} + kr \tag{1.3}$$

Where the first term is asymptotic freedom due to single gluon exchange and the second one is quark confinement term. The non-relativistic treatment only describe the feature of charmonium levels.

The potential description extended to the spin-dependent regime by adding three interaction term to the above potential describe below,

$$V(r) = V_{LS}(r)(\vec{L}.\vec{S}) + V_T(r)[S(S+1) - \frac{3(\vec{S}.\vec{r})((\vec{S}.\vec{r})}{r^2}] + V_{SS}(r)[S(S+1) - \frac{3}{2}] \tag{1.4}$$

where V_{LS} is spin-orbit term, V_T describes fine structure, and V_{SS} spin-spin term gives the spin singlet splitting. The spin-spin contact hyperfine interaction is one of the

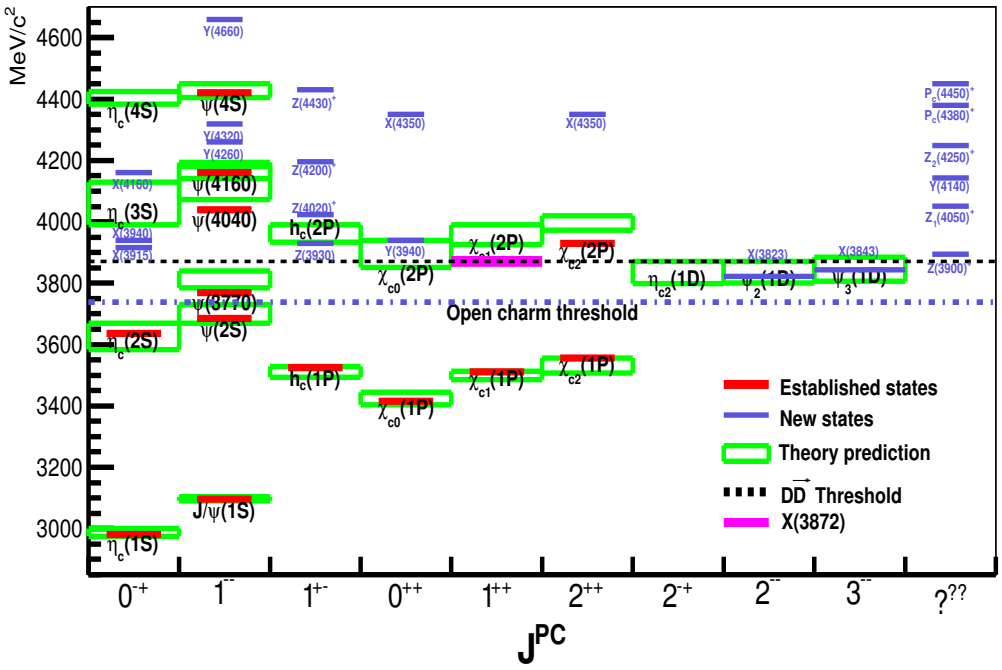

Figure 1.1: Charmonium spectrum comparing theory and experiment.

spin-dependent terms predicted by one gluon exchange forces. Other spin-dependent

terms are treated as mass shifts using the leading-order perturbation theory. From this potential one can get information (mass, charge, parity, etc.) regarding charmonium states.

Comparison between experimentally observed spectrum and the predictions of conventional $c\bar{c}$ model is shown in Fig 1.1. There is a remarkable agreement between experiment and theory below open charm threshold of $D\bar{D}$. However, we can see a discrepancy between experiment and theory above the $D\bar{D}$ threshold. Further, many new states have found which suggest that our understanding of charmonium states is minimal. Input from theory and experiment is needed to improve our knowledge about charmonium.

1.4 Charmonium production

Charmonium produces in many ways. In this thesis, only the processes (important ones) through which charmonium produce at the B-factories has explained.

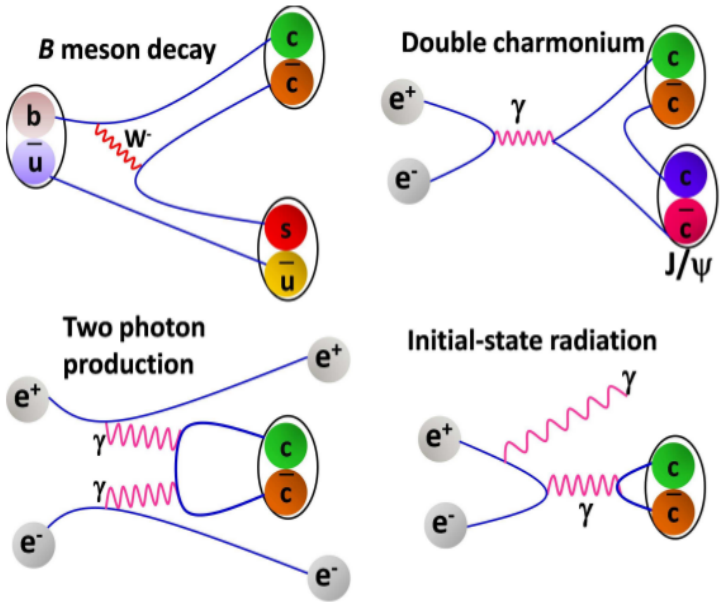

Figure 1.2: The processes which are responsible for charmonium production.

- B meson decay

  The decays of the B meson provides a clean production environment for charmonium. Almost 15% charmonium produce from B meson decaying into K

meson. As charge parities do not conserve in weak decays, charmonium with any quantum number provides in the two-body decays. Large $\Upsilon(4S)$ data at KEK-B factory provides an excellent environment to study these states and find new resonances.

- Two-photon production

  Electron-positron annihilation at higher energies can produce charmonium states through two virtual photons via the process

$$e^+e^- \rightarrow e^+e^- + (c\bar{c}) \tag{1.5}$$

  when high energy e^+ and e^- are coming to each other they radiate photons which interact with each other. A charmonium state appearing in the two-photon collision has positive C-parity.

- Initial state radiation

  In this process either the electron or the positron radiates a photon before the annihilation, thereby lowering the sufficient CM energy. Only J^{PC}=1^{--} produce through initial state radiation.

- Double charmonium

  The production of double charmonium states in e^+e^- annihilation discovered by the Belle collaboration from a sample of data collected near the $\Upsilon(4S)$resonance at a CM energy 10.6 GeV. In the process of pair charmonium production in e^+e^- annihilation, the final charmonium states have opposite charge parities.

1.5 Charmonium like exotic states

In recent years, particles have found like $X(3872)$, $X(3915)$, $Y(4260)$, etc., whose resemble like charmonium but seems to have different properties than conventional charmonium states. They fall in the category of charmonium like or exotic states. These exotic states broadly classified into three models: Multiquark, charmonium hybrid, structure due to threshold effects.

1.5.1 Multiquark

All known hadrons categorize as either meson, formed of a quark and an antiquark, or baryons, formed of three quarks (or the antimatter equivalent). There are other quark combinations possible, known as multiquark structure. The molecular state (also known as deuson) which comprises of two charmed mesons bound together to form a molecule. Molecular states are loosely bound and are expected to bind through two mechanisms: quark/color exchange interactions at a short distance and pion exchange at large distance. $X(3872)$ mass is very close to the sum of the masses of the D^0 and $\bar{D^{*0}}$ mesons. It speculated that $X(3872)$ could be a D^0 and $\bar{D^{*0}}$ loosely bound state.

Multiquark state can also exist in the form of a tightly bound four-quark state (known as tetra-quark), and they are expected to have properties different from those of a molecular state. Tetra-quark describes as a diquark-antiquark structure in which the quarks group into color-triplet scalar and vector clusters and the interactions dominates by simple spin-spin interaction. In tetraquark hypothesis for $X(3872)$, a mass splitting due to mixing between $c\bar{c}u\bar{u}$ and $c\bar{c}d\bar{d}$ is predicted.

1.5.2 Charmonium Hybrid

Hybrid mesons are states which have an exciting gluon degree of freedom.

1.5.3 Structure due to Threshold Effects

In addition to these states, the threshold can also give rise to the structures in cross sections and kinematics distributions. The possible threshold includes DD^*, D^*D^*, DD_1 and D^*D_1 at centre of mass energy 3872, 4020, 4287 and 4430 MeV, respectively.

1.6 $X(3872)$ state

Last decade has been very exciting for the quarkonium sector. Many new states have found which find no place in the conventional spectroscopy and are a strong contender of the exotic quarkonium states (tetra-quark, molecular, hybrid). $X(3872)$

has remained to be the poster boy of these exotic states, from the time the Belle Collaboration first observed it in 2003 [1].

$X(3872)$ has also seen to decay into other final states: $X(3872) \to D^0\bar{D}^{*0}$, $X(3872) \to J/\psi\gamma$, $X(3872) \to \psi'\gamma$ and $X(3872) \to J/\psi\pi^+\pi^-\pi^0$ [2, 3, 4, 5, 6]. Recently, BESIII observed $X(3872) \to \chi_{c1}\pi^0$ decay mode using $e^+e^- \to (\chi_{c1}\pi^0)\gamma$ [7]. Negative C-odd partner search of $X(3872)$ ($X(3872) \to J/\psi\eta$ [8], $X(3872) \to \chi_{c1}\gamma$, $X(3872) \to \eta_c\omega$, $X(3872) \to \eta_c\pi\pi$ [9]) and charged partner search $X(3872)^+ \to J/\psi\pi^+\pi^0$ [10] suggest that $X(3872)$ is an iso-singlet state.

If so then its decay into its discovery mode $X(3872) \to J/\psi\pi^+\pi^-$ is expected to be an isospin not allowed. Further, one expect the decay $X(3872) \to J/\psi\pi^+\pi^-\pi^0$ to be an isospin allowed and should have large branching fraction, something like $R_{3\pi/2\pi} \equiv \mathcal{B}(X(3872) \to J/\psi\pi^+\pi^-\pi^0)/\mathcal{B}(X(3872) \to J/\psi\pi^+\pi^-) \sim 30$ [11]. However, the previous measurement by the Belle with 256 fb^{-1} data suggest $R_{3\pi/2\pi}$ to be $1.0 \pm 0.4 \pm 0.3$ [12]. Measurement by the BaBar Collaboration using their full data set 426 fb^{-1} gave this number as 0.8 ± 0.3 [13]. Recently BESIII measured $R_{3\pi/2\pi}$ to be $1.6^{+0.4}_{-0.3}\pm0.2$ in $e^+e^- \to \gamma J/\psi\omega$ (X(3872)$\to$ J/$\psi\omega$) decay [14]. This suggest large isospin violation, which is not properly understood. Belle accumulated 711 fb^{-1} data, almost twice of BaBar. Updating this ratio will give a more precise measurement.

Chapter 2

Experimental Setup

2.1 Introduction

To observe the CP violation in the $B\bar{B}$ system and to determine the CKM matrix elements, two B-factories were proposed one at KEK (High Energy Accelerator Research Organisation), Japan and another at PEP at SLAC, the USA in 1994, Table 2.1. The B-factory at KEK is known as KEK B-factory. The data used to perform this analyses has been collected at KEKB e^+e^- asymmetric collider using the Belle detector, at High Energy Accelerator Research Organization, KEK, Japan. In this chapter, an explanation of KEKB accelerator and Belle detector components has given. It provides a clean and excellent environment to study B physics, charmonium like states and CP violation in B-meson system.

2.2 KEKB Collider

The KEKB is an asymmetric energy e^+e^- collider with e^- having energy 8 GeV and e^+ having energy 3.5 GeV. The center-of-mass (CM) energy $\sqrt{s}$ of this e^+ e^- collision at KEK B-factory is

$$\sqrt{s} = \sqrt{4E_{e^+}E_{e^-}} = 10.58 \text{ GeV}. \tag{2.1}$$

which is equal to the mass of $\Upsilon(4S)$ resonance. The $\Upsilon(4S)$ mainly decays to $B^0\bar{B}^0$ or B^+B^- in almost equal amount. Since the energy of e^+ and e^- is asymmetric, so

the B-meson pairs are created with a Lorentz boost factor of

$$\beta\gamma = \frac{E_{e^-} - E_{e^+}}{\sqrt{s}} = 0.425. \tag{2.2}$$

Since the branching fractions of the B decays are very small, so large number of B mesons are necessary for the CP violation studies. The design luminosity of KEKB machine is 1×10^{34} cm^{-2}s^{-1} which corresponds to the production of 10^8 B mesons per year.

Table 2.1: B-factories in the world.

Institute	Accelerator	Type	Detector	Year
Cornell	CESR	e^+e^- sym.	CLEO II, III	1995 – 2001
SLAC	PEP-II	e^+e^- asym.	BaBar	1999 – 2008
KEK	KEK-B	e^+e^- asym.	Belle	1999 – 2010
DESY	HERA	fixed (p+wires)	HERA-B	1999 – 2003
CERN	LHC	pp	LHCb	2007 –
KEK	SuperKEK-B	e^+e^- asym.	Belle II	2010 –

2.3 KEKB Accelerator

The configuration of the KEKB storage ring has shown in Figure 2.1. To generate the Lorentz boosted B meson pairs, KEKB is designed to be an asymmetric energy e^+e^- collider consisting of two rings. The ring for e^- having energy 8 GeV called high energy ring (HER) while for e^+ having energy 3.5 GeV is called low energy ring (LER). In the first stage of the linac, electrons accelerated to an energy of 4 GeV. Positrons produce by hitting a thin tungsten mono-crystal target with some of these electrons, which will radiate photons. These photons further create electron-positron pairs. Out of these, positrons are collected and accelerated to 3.5 GeV. The electron beam is then accelerated also to 8 GeV, and both axles directly injected into the rings at full energies (3.5 GeV and 8 GeV respectively for LER (e^+) and HER (e^-)).
In its whole life, it has delivered more than 1040.86 fb^{-1} data and belle has acquired data of $1014 fb^{-1}$ which divided into data sets of Table 2.2.

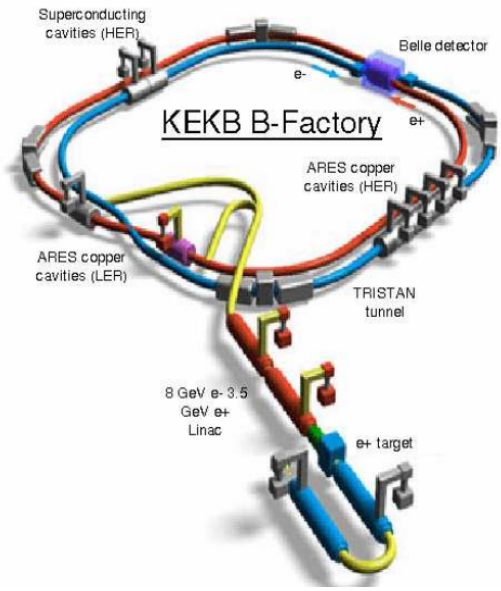

Figure 2.1: Schematic diagram of the KEKB accelerator.

Table 2.2: Accumulated data set at Belle.

Resonance	Luminosity (fb^{-1})
$\Upsilon(1S)$	6
$\Upsilon(2S)$	24
$\Upsilon(3S)$	3
$\Upsilon(4S)$	711
$\Upsilon(5S)$	121
Off reson./scan	$\sim$ 100

2.4 The Belle Detector

Construction of Belle detector mainly aims to carry out a quantitative study of B meson decays and in particular rare B decay modes with tiny branching fraction. B mesons are very short-lived particles and decay almost instantaneously into relatively long lifetime particles before they reach the innermost detector. The Belle detector detects these particles namely, $e^{\pm}$, $\mu^{\pm}$, $\pi^{\pm}$, $K^{\pm}$, p, $\bar{p}$, γ, and K^0. Figure 2.2 describes the Belle detector and its sub-detectors. The sub-detectors are

- Silicon vertex detector (SVD)
- Central drift chamber (CDC)
- Aerogel cerenkov counter (ACC)
- Time of flight scintillator(TOF)
- Electromagnetic calorimeter(ECL)

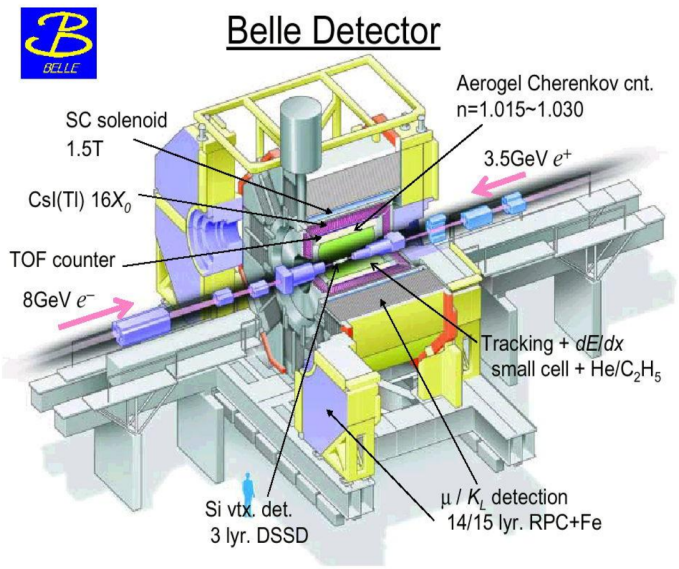

Figure 2.2: Schematic diagram of the Belle detector.

- Kaon and muon datector(KLM)
- Extreme forward calorimeter(EFC)

helps to detect long life elementary particles.

2.4.1 Beam Pipe

Beam pipe is the inner-most part of the Belle detector and all the particles transverse through it before reaching the SVD.

2.4.2 Silicon Vertex Detector (SVDI)

The SVD provides a precise measurement of the decay vertices of B-mesons. It helps to measure the flight length of the produced B mesons in z-direction with precise measurement ($\sim$ 100 μm) and contributes to the track reconstruction of charged particles which helps to improve the momentum resolution of the particles.

SVDII

New SVD (SVDII) installed in the summer of 2003. There are many improvements in this one as compared to SVDI. The geometrical configuration of SVDII has shown

in Figure 2.3. For SVDII, the radius of the beam pipe has been reduced to put silicon closer to interaction point and to achieve better vertex resolution.

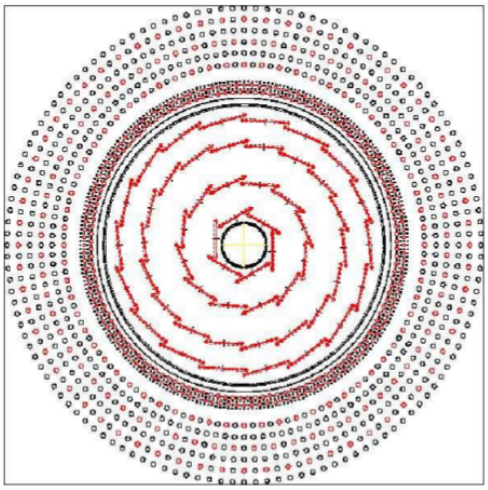

Figure 2.3: silicon vertex detector (SVDII).

2.4.3 Central Drift Chamber (CDC)

The determination of three-dimensional trajectories of charged particles and precise measurement of their momenta is the main motive of Central Drift Chamber (CDC). The 1.5 T magnetic field of superconducting solenoid bends the charged particle according to their momenta. Also, the CDC is used to measure the energy loss (dE/dx) of charged particles for their particle identification. The CDC is involved in the particle identification for the tracks with momentum $p < 0.8$ GeV/c and $p > 2.0$ GeV/c measuring dE/dx.

2.4.4 Aerogel $\check{C}$erenkov Counter (ACC)

Particle identification, specifically the identification of $\pi^{\pm}$ and $K^{\pm}$ plays an important role in the B mesons system as well as for our analysis decay modes. In the momentum region below 1 GeV/c, the K/π separations performed by dE/dx measurement from CDC and time of flight measurements. The ACC provides the K/π separation in momentum range of $1.2 < p < 3.5$ GeV/c by detection of the $\check{C}$erenkov light from particle penetrating through silica aerogel radiator.

2.4.5 Time of Flight Counter (TOF)

The TOF detector works on the principle of scintillation: the property of certain chemical compounds to emit short light pulses after excitation by the passage of charged particles or by photons of high energy. The counters measure the elapsed time between a collision at the interaction point and the time when the particle hits the TOF layer. For the measured flight time (T) from TOF, and measured flight length and momentum by CDC track fit, one can estimate the mass of each track in an event.

2.4.6 Electromagnetic Calorimeter (ECL)

The ECL is designed to measure the energy and position of photons and electrons produced in Belle. The main purpose of Electromagnetic Calorimeter (ECL) is the detection of photons and electrons with high efficiency and good resolutions in energy and position.

In addition to the measurement of the energy of photons and electrons, the ECL plays an important role in electron identification. The following information helps to detect electrons: Matching between the position of the charged track measured by the CDC and that of the energy cluster measured by the ECL.

- E/p, i.e., the ratio of energy measured by the ECL to momentum measured by the CDC.
- E_9/E_{25} at the ECL, i.e., the ratio of ECL shower energy in an array of 3×3 crystals to the energy in an array of $5\times$ five crystals.
- dE/dx measured by CDC.
- Light yield in the ACC.
- Time-of-flight measured by TOF.

2.4.7 K_L/μ Detector (KLM)

To identify K_L^0's and muons with efficiently and low fake rate over a broad momentum range above 600 MeV/c, the K_L/μ Detector (KLM) has designed. The K_L^0 particles live long enough and travel beyond the ECL and interact primarily via the strong force. Detection of them performed by hadronic showers of ionizing particles to which they decay.

2.4.8 Extreme Forward Calorimeter (EFC)

In order to improve the experimental sensitivity to physics processes, the extreme forward calorimeter (EFC) is needed to extend the polar angle coverage by ECL, $17^o < \theta < 150^o$. The EFC covers angular range from $6.4^o < \theta < 11.5^o$ in the forward direction and $163.3^o < \theta < 171.2^o$ in the backward direction.

2.5 Data samples

- **Experimental Data**

  The present analysis is based on the Belle full data sample of 711 fb^{-1} recorded at the $\Upsilon(4S)$ resonance. This data sample corresponds to $(771.6 \pm 10.6) \times 10^6 B\bar{B}$ pairs, referred to as $B\bar{B}$ events.

- **Simulated Data**

  For a particular B-meson decay mode, the analysis procedure was established using Monte Carlo (MC) simulated events. The Software program packages EvtGen [15] is used to simulate the decay processes, while the Belle detector response is simulated using geant 3.4 software. 1 Million simulated signal events are generated each decay mode. The simulated samples are used to implement and test the event reconstruction and study reconstruction efficiencies.

2.6 Detection of different particles for the concerned decay modes

Table 2.3: Sub-detectors which detect different particles.

Particle	Energy	Momentum	Position	Particle Identification
$e^+(e^-)$	ECL	CDC	SVD, CDC	ECL, ACC, TOF, CDC
$\mu^+(\mu^-)$		CDC	SVD, CDC	KLM, ACC, TOF, CDC
$\pi^+(\pi^-)$		CDC	SVD, CDC	ACC, TOF, CDC
$K^+(K^-)$		CDC	SVD, CDC	ACC, TOF, CDC
γ	ECL		ECL	ECL, CDC

Due to short life time of B-meson, it is not detected directly in Belle detector. This detector will be able to detect final state (fairly stable) particles like e, μ, π, K, γ etc. In Table 2.3, we have mentioned how detection of different particles takes place for our concerned decay modes by different sub-detectors.

Chapter 3

Analysis

3.1 Introduction

In this chapter, the analysis procedure of $B^{\pm} \to X(3872)K^{\pm}$ and $B^{\pm} \to X(3915)K^{\pm}$ decay mode has been explained, where $X(3872)$ and $X(3915)$ decays to $J/\psi\omega$. BaBar found the evidence for $X \to J/\psi\omega$ decay mode in 426 fb^{-1} data and measured the $R_{3\pi/2\pi}$ ratio to be 0.8±0.3[13]. Recently BESII measured the ratio to be 1.6±0.2, little bit higher value[14]. The verification and improved measurement of this decay mode still awaited, as this decay mode are of great interest for the theoretical understanding of the newly discovered charmonium state $X(3872)$. Using a large amount of Belle data set, which is almost two times the size of data of BaBar, have a great chance to measure this ratio perfectly and to get a better understanding the nature of $X(3872)$.

3.2 Signal Monte Carlo

We generated 1 Million signal MC events (experiment dependent run independent) for the following decay modes:

- $B^+ \to X(3872)K^+$, $X(3872) \to J/\psi\omega$, $\omega \to \pi^+\pi^-\pi^0$ [16].
- $B^0 \to X(3872)K^0_S$, $X(3872) \to J/\psi\omega$, $\omega \to \pi^+\pi^-\pi^0$ [16].
- $B^+ \to X(3915)K^+$, $X(3915) \to J/\psi\omega$, $\omega \to \pi^+\pi^-\pi^0$ [16].

- $B^0 \to X(3915)K^0_S$, $X(3915) \to J/\psi\omega$, $\omega \to \pi^+\pi^-\pi^0$ [16].

For this purpose we have used EvtGen generator [15]. Detector response is followed by detector simulation software GSIM based on Geant3.4 [17]. Decay chain for $B^\pm \to X(3872)K^\pm$, $B^0 \to X(3872)K^0_S$, $B^\pm \to X(3915)K^\pm$ and $B^0 \to X(3915)K^0_S$ is as follows:

$$e^+e^- \to \Upsilon(4S) \to B\bar{B},\ B \to \text{decay of interest (Fig 3.1)}.$$

We used PHOTOS to take care of the initial and final state radiation.

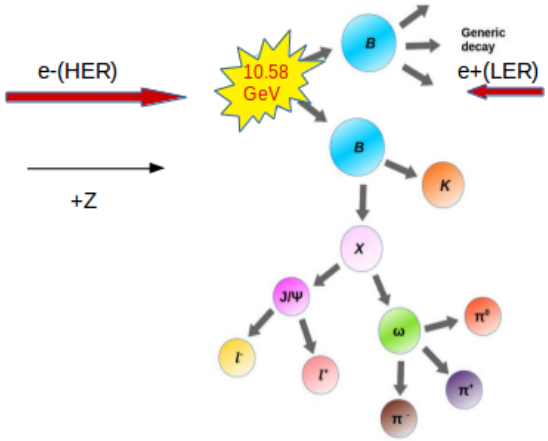

Figure 3.1: The main decay scheme.

3.3 Particle Identification

B meson is reconstructed from it's decay products. The particles used to reconstruct B meson are $e^\pm$, $\mu^\pm$, $\pi^\pm$, $K^\pm$, and γ. These are the final particles which are detected by the detector needed to reconstruct our decay mode of interest.

3.3.1 Basic cuts and criterion's

The Belle data consists of a large number of events which not only comes from $e^+e^- \to \Upsilon(4S) \to B\bar{B}$ but also from several other processes such as τ pair, Bhabha, continuum events $e^+e^- \to q\bar{q}$ (where q stands for u, d, s and c), two-photon, and beam gas interactions, which occur with similar or larger cross sections than $B\bar{B}$ production.

In this study, we are interested only in the events coming from the $B\bar{B}$ events (where one of the B has $J/\psi \to \ell^+\ell^-$ in the final state of the decay). So, we use the `psiskim` data ($772 \times 10^6 B\bar{B}$ pairs) based on HadronBJ event selection provided as the `caseB` data [18].

B and $X(3872)$ states are reconstructed using the following decay process:

$$B \to X(3872)K,\ X(3872) \to J/\psi\omega,\ J/\psi \to \ell^+\ell^-,\ \omega \to \pi^+\pi^-\pi^0 \tag{3.1}$$

Here ℓ is e or μ. K stands for $K^\pm$ and K^0_S. To suppress the background coming from the continuum events ($e^+e^- \to q\bar{q}$), ratio of second to zeroth Fox-Wolfram moments is used [19].

$$R_2 = \frac{H_2}{H_0} \tag{3.2}$$

$$H_k = \sum_{i,j} \mid p_i \mid p_j \mid P_k(\cos\theta_{ij}) \tag{3.3}$$

Here p_i is the four momentum of i-th track $\cos\theta_{ij}$ is the angle between i-th and j-th tracks. P_k is the Legendre polynomial.

Produced B mesons are at rest, and their decay axis is uncorrelated. So, $B\bar{B}$ events are spherical in shape and can be distinguished from jet-like continuum events of u, d, s or c. R_2 is zero for the spherical events. R_2 parameter has chosen less than 0.5 to reduce continuum background. Good tracks are having a distance of closest approach to interaction point (IP) in the beam direction (z) of less than 3.5 cm and less than 1.0 cm in the transverse plane (xy-plane), shown in Fig 3.2.

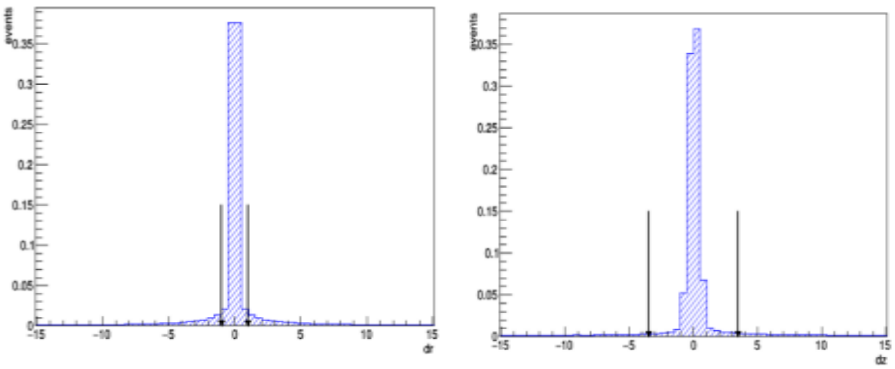

Figure 3.2: Distribution of dr (left) and dz (right) for the tracks (normalized to unity) from signal MC, with arrows showing the cuts used in the analysis.

3.3.2 K/π selection

Charged K and π selection is based on the information from ACC (number of Cherenkov photons), TOF (time of flight measurement) and CDC (dE/dx measurement) from detectors. The pion (kaon) identification is based upon the likelihood ratio, which is defined as:

$$\mathcal{R}(K) = \frac{\mathcal{L}(K)}{\mathcal{L}(\pi) + \mathcal{L}(K)}. \tag{3.4}$$

Charged kaons (pions) are identified by equiring the $\mathcal{R}(\mathrm{K}) > 0.6$ ($\mathcal{R}(\pi) > 0.6$). $\mathcal{R}(\mathrm{K})$ distribution shown in Fig 3.3.

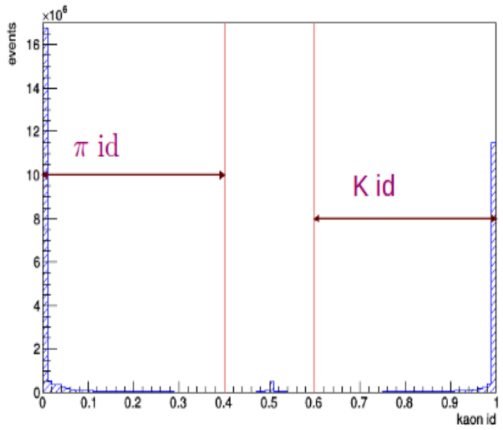

Figure 3.3: $\mathcal{R}(\mathrm{K})$ distribution with cuts used to identify π and K candidate from signal MC.

3.3.3 μ, e selection

Using the information of track penetration depth from the KLM system muons are identified. Electrons are identified using E/p ratio (energy, E from ECL and momentum, p from CDC and SVD) and $\Delta E/dx$ from CDC.

3.3.4 γ selection

In Belle detector, γ candidate is based upon their EM interactions inside the ECL (a shower production mechanism). Selection criteria applied on the EM shower is $\frac{E_9}{E_{25}} > 0.85$, where E_9 (E_{25}) is the energy deposited in the 3x3 (5x5) crystals in the ECL.

3.4 Reconstruction

Using the identified final states, intermediate and primary states can be reconstructed.

3.4.1 π^0 reconstruction

Reconstruction of neutral pions has done by combining two photons with energy greater than 60 MeV. To reduce combinatorial background, the $\pi^0 \to \gamma\gamma$ candidates are also required to have an energy balance parameter $\frac{|E_1-E_2|}{(E_1+E_2)}$ smaller than 0.8, where $E_1(E_2)$ is the energy of the first (second) photon in the laboratory frame. By comparing π^0 mass in MC, it's clear that $\pm 2\sigma$ cut can be applied to select the π^0 more efficiently. In Fig 3.4, we can see that the signal efficiency increased by applying a 2σ cut. Thus we can remove fake π^0 candidates. The π^0 candidates are identified as 123 MeV/c^2 $< M_{\pi^0} <$ 147 MeV/c^2.

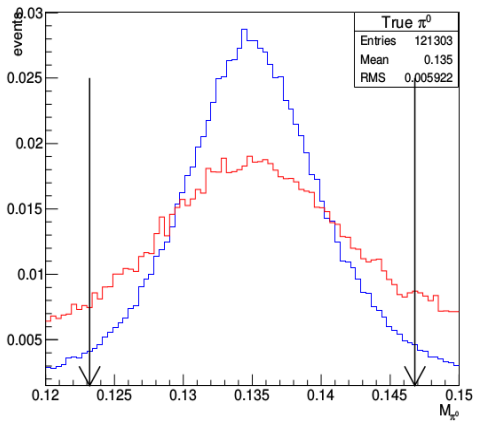

Figure 3.4: The blue distribution is the truth matched π^0 candidates, while the red histogram represents the mis-reconstructed fake π^0 candidates from signal MC. The arrow lines demonstrate the cut used in analysis. We selected 123 MeV/c^2 $< M_{\gamma\gamma} <$ 147 MeV/c^2 for further usage.

3.4.2 ω from pions

ω is reconstructed from its decay particles π^+, π^- and π^0. Fig 3.5 shows the reconstructed invariant mass of $M(\pi^+\pi^-\pi^0)$. Among the reconstructed candidates ω is identified as 0.700 GeV/c^2 $< M_\omega <$ 0.850 GeV/c^2 for further usage.

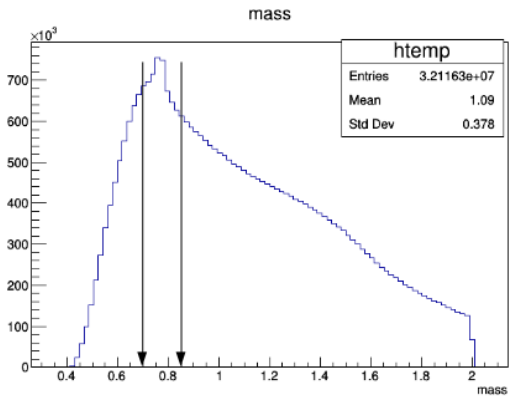

Figure 3.5: Distribution of of $M_{\pi^+\pi^-\pi^0}$ (in GeV/c^2) from signal MC, arrows showing the selected ω candidates for further processing.

ω selection optimization

If a particle decays into three daughters, then its kinematics can be described by the Dalitz plot. We utilized the ω Dalitz plot for rejecting fake events and selecting true events. For a three-body decay, there are total 12 parameters (3, four-momentum) out of which two independent (10 constraints: 4 conservation of momentum, three masses, 3 Euler angles). These two independent parameters are described by,

$$X = \frac{\sqrt{3}(T_{\pi^+} - T_{\pi^-})}{Q} \tag{3.5}$$

$$Y = \frac{2T_{\pi^0} - (T_{\pi^+} + T_{\pi^-})}{Q} \tag{3.6}$$

where T_{π^0}, T_{π^+}, T_{π^-} are kinetic energy of π^0, π^+, π^- respectively, and $Q = T_{\pi^0} + T_{\pi^+} + T_{\pi^-}$ is the energy release in the decay. Fig 3.6 shows the Dalitz distribution for the ω decay after truth matching. As clearly see from Fig 3.6, the concentration of true signal events at the central region of the triangle is much higher than corner region, while the fake events tends to concentrate more on the side of the Dalitz plot. Therefore, we use two concentric circular cut for selecting best omega candidates. We are selecting region between two concentric circle. Equation of two circles are,

$$(X - x_1)^2 + (Y - y_1)^2 = R_1^2 \tag{3.7}$$

$$(X - x_1)^2 + (Y - y_1)^2 = R_2^2 \tag{3.8}$$

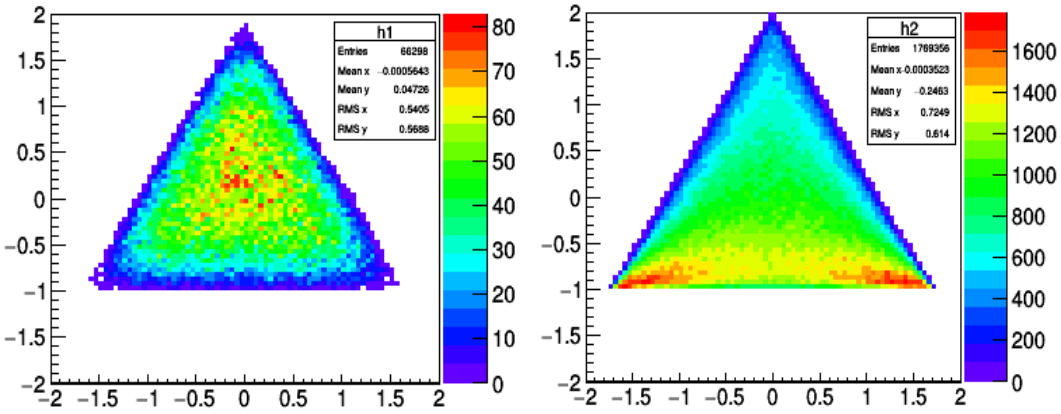

Figure 3.6: Dalitz plot for the $\omega \to \pi^+\pi^-\pi^0$ decay from signal MC. Left distribution is for the truth matched signal events while the right one is for the truth matched fake events in $B^\pm \to X(3872)K^\pm$ decay.

Here, (x_1, y_1) is the common centre, while R_1 and R_2 is the centre of the inner and outer circle, respectively. After checking efficiency of various circular cuts we have selected the cut centered at (0,3) with region of radius in between $R_1 = 1.5$ and $R_2 = 3.8$. This corresponds to reduction of fake events by 29 % and signal rejection of 7 %. Selected events (represented with the contour) are projected on the signal and background separately shown in Fig 3.7. We are selecting the same cut for $B^0 \to X(3872)K^0$, $B^\pm \to X(3915)K^\pm$ and $B^0 \to X(3915)K^0$ decay mode.

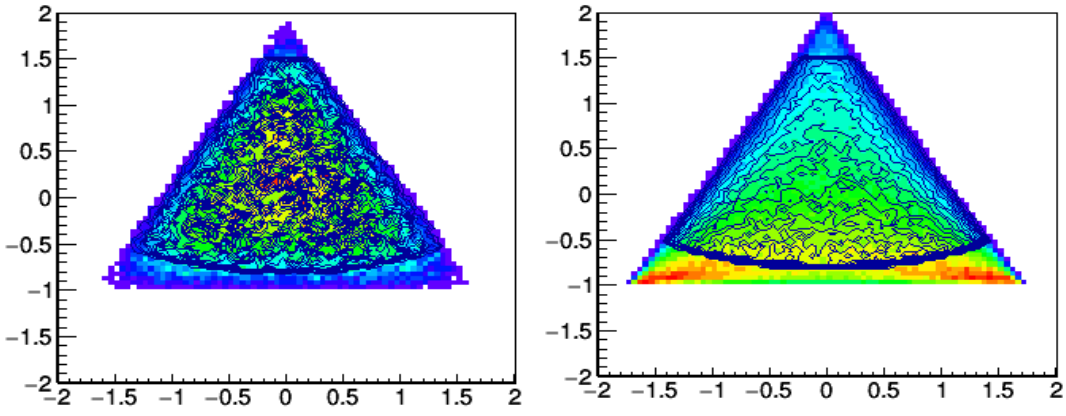

Figure 3.7: Dalitz plot for the $\omega \to \pi^+\pi^-\pi^0$ decay after applying cut from signal MC. Left distribution is for the truth matched signal events while the right one is for the truth matched fake events in $B^\pm \to X(3872)K^\pm$ decay. Selected events are projected on signal and backgrounds respectively.

3.4.3 Reconstruction of J/ψ

J/ψ is reconstructed using $\ell^+\ell^-$, where ℓ is electron and muon. Different cuts are used to select the J/ψ candidates for e and μ. The cut corresponding to $J/\psi \to \mu^+\mu^-$ is 3.07 GeV/c^2 < $M_{\mu\mu}$ <3.13 GeV/c^2. There is a loss of energy from the electron in the form of emission of bremsstrahlung photons. The four momenta of the photons within 0.05 radian of e^+ or e^- direction are included in the invariant mass calculation. However, even after this correction, the $J/\psi \to e^+e^-$ signal shape is still skewed Fig 3.8, which is taken into account by using an asymmetric invariant mass window 3.05 GeV/c^2 < $M_{ee\gamma}$<3.13 GeV/c^2 to define J/ψ candidate in the electron channel. J/ψ candidates are selected with momentum less than 2 GeV/c^2 to avoid direct J/ψ coming from B meson decay.

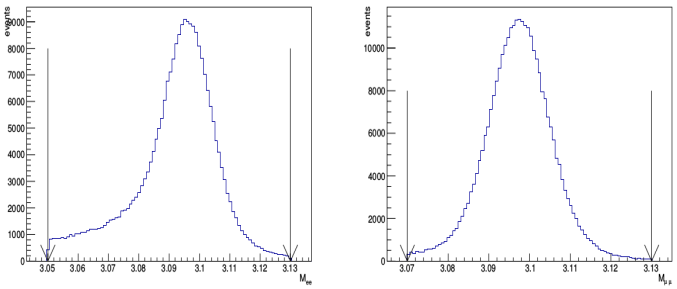

Figure 3.8: J/ψ reconstruction from e^+e^-(left) and $\mu^+\mu^-$(right) from signal MC.

3.4.4 Reconstruction of $X(3872)$, $X(3915)$ and B

The reconstruction of $X(3872)$ and $X(3915)$ are done through their decays to $J/\psi\omega$, $\omega \to \pi^+\pi^-\pi^0$. Subsequently, reconstruction of B meson has done by combining

- $X(3872)$ candidates and K candidates for $B \to X(3872)K$ decay mode.
- $X(3915)$ candidates and K candidates for $B \to X(3915)K$ decay mode.

Here K can be $K^\pm$ and K^0_S.

Kinematical variables

To identify the B meson, two kinematical variables are used : beam constrained mass and energy difference.

- The beam constrained mass ; $M_{\rm bc}$ is defined as $\sqrt{E^2_{\rm beam} - \sum_i p_i^2}$.
- Energy difference (ΔE) is defined as $\sum_i E_i - E_{\rm beam}$.

Here $E_{\rm beam}$ is the beam energy in the center of mass (cm) frame and p_i (E_i) is the momentum (energy) of the i-th particle in the cm frame of the $\Upsilon(4S)$ and summation is over all of the final states used for reconstruction. The grand selection for B meson candidates are taken as -0.2 GeV <ΔE <0.2 GeV (later we will optimized it) and M_{bc} >5.2 GeV/c^2 region, shown in Fig 3.9. signal window for M_{bc} is defined as M_{bc}>5.27 GeV/c^2.

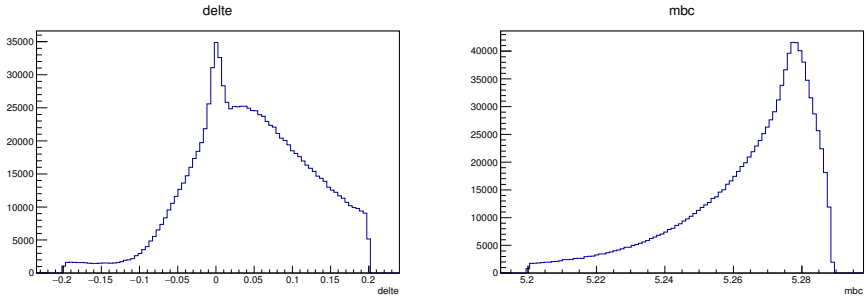

Figure 3.9: Distribution of ΔE (left) and M_{bc} (right) for the $B^{\pm} \to X(3872)(J/\psi\omega)K^{\pm}$ decay mode from signal MC.

Best Candidate Selection

After applying the selection criteria as mentioned above, we find that in the signal region around 35% of the total events having multiple B candidates. Which arises due to wrong combinations or missing particles. Fig 3.10 shows B candidate multiplicity for $B^{\pm} \to X(3872)K^{\pm}$ decay mode from signal MC. One expect one B candidate per

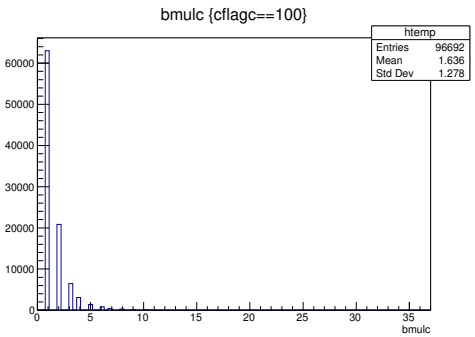

Figure 3.10: Number of B candidates for $B^{\pm} \to X(3872)K^{\pm}$ decay mode from signal MC.

event. In order to select the best candidate among them, two methods were tested.

1. M_{bc} closest to the nominal B value.

Among the multiple B meson candidates, the one with M_{bc} value closest to the PDG value of B mass is selected.

2. χ^2 fitting. Where

$$\chi^2 = \chi^2_V + (\frac{M_{ll} - m_{J/\psi}}{\sigma_{J/\psi}})^2 + (\frac{M_{\pi^+\pi^-\pi^0} - m_\omega}{\sigma_\omega})^2 + (\frac{M_{\gamma\gamma} - m_{\pi^0}}{\sigma_{\pi^0}})^2 + \chi^2_{\Delta E} + (\frac{M_{\pi^0\pi^0} - m_{K_s}}{\sigma_{K_s}})^2. \tag{3.9}$$

M is the reconstructed mass and m is the PDG mass value. σ is the mass width and χ^2_V is obtained by vertex fitting of all the charged tracks. Similarly χ^2 values for ΔE, masses of J/ψ, ω, π^0, K_s are obtained and summed. For both cases BCS efficiency and multiplicity are calculated. BCS efficiency and multiplicity are defined as,

Multiplicity = Number of events having multiple candidate in total event.

BCS efficiency = (Number of true signal events selected in BCS with multiplicity > 1)/(Number of true signal events having multiplicity > 1).

Table 3.1 compares the BCS efficiency and multiplicity for the two methods described above. By looking at Table 3.1, we can say that BCS efficiency is more for min χ^2. Therefore, we used this method for the best candidate selection.

Best Candidate Selection			
Selection type	Signal candidate	BCS efficiency(%)	Multiplicity(%)
$M_{\rm bc}$	$B^\pm \to X(3872)K$	59.1	34.9
	$B^0 \to X(3872)K^0_S$	51.5	37.1
min χ^2	$B^\pm \to X(3872)K$	68.5	34.9
	$B^0 \to X(3872)K^0_S$	56.7	37.1

Table 3.1: BCS efficiency and multiplicity

3.5 ΔE optimization

The reconstructed event can be signal or background. To remove maximum background with less signal loss, we optimize the selection window for ΔE, so that the figure of merit (FoM) value is maximum.

$$FoM = \frac{N_{sig}}{\sqrt{N_{sig} + N_{bkg}}} \tag{3.10}$$

N_{sig} is the yield of expected signal events from signal MC and N_{bkg} represents that of background estimated from $B \to J/\psi X$ inclusive MC sample. For calculating N_{sig} we used the PDG branching fraction for $(B \to XK, X \to J/\psi\omega)$ decay (we used 6.0×10^{-6} when $X = X(3872)$ and 3.0×10^{-5} when $X = X(3915)$).

One expect signal events will have a ΔE value close to zero. Therefore the lower bound of the ΔE selection window should be a negative and upper bound a positive. To find the lower bound, an arbitrary positive value is chosen and a negative value varied from -0.2 to 0 GeV is be taken. The events which fall in these intervals (windows) were considered and the FoM values were calculated for each intervals. Then FoM versus negative ΔE value graph was plotted and the ΔE with maximum FoM value was taken as lower bound. Similar process has done with to obtain the upper bound of ΔE window, by fixing the lower bound. The ΔE region obtained through this method is -0.02 < ΔE < 0.02 GeV/c^2, Fig 3.11.

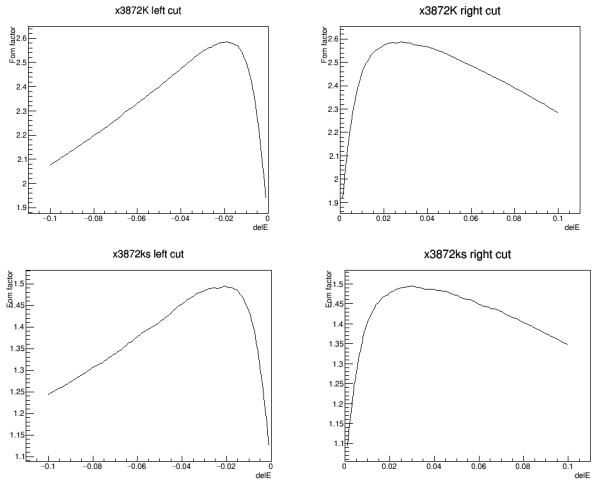

Figure 3.11: Figure of merit (FoM) for ΔE < 0 (left) and ΔE > 0 (right). For $B^{\pm} \to (X3872)K^{\pm}$(top) and for $B \to X(3872)K_s$(bottom)

3.6 Background Study

3.6.1 Inclusive MC

To study the possible sources of background, $B \to J/\psi X$ inclusive MC samples are analyzed(100x data). Since we are interested in $X(3872) \to J/\psi\omega$, the invariant mass $M_{J/\psi\omega}$ is checked. From Fig 3.12 (right), one can clearly see that most of the $B \to$

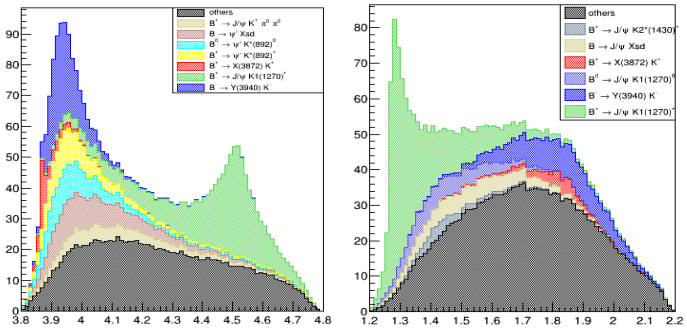

Figure 3.12: Major peaking backgrounds along with signals in $M_{J/\psi\omega}$(left) and $M_{K\omega}$(right) distribution from inclusive MC.

$J/\psi K_1(1270)^+$ decay events can be removed by applying $M_{K\omega} > 1.4$ GeV/c^2. After applying the cut, $M_{J/\psi\omega}$ plot shown in Fig 3.13, this helps in removing background from the higher K* resonances.

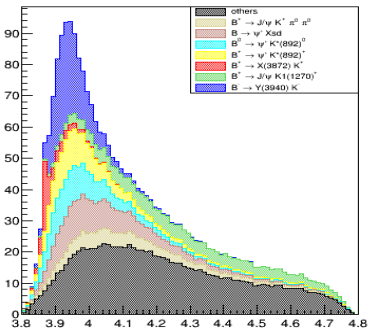

Figure 3.13: Major peaking backgrounds along with signals in $M_{J/\psi\omega}$ distribution after applying $M_{K\omega}$ cut from inclusive MC.

3.7 Resolution Improvement techniques

3.7.1 Modification of π^0 momentum

Ideally ΔE should be zero for perfect reconstruction. If one assume that the resolution of ΔE is poor due to poorly reconstructed π^0, one can scale the energy of π^0 as (Fig 3.14)

$$s = \frac{E_{beam} - (E_{J/\psi} + E_{\pi^+} + E_{\pi^-} + E_K)}{E_{\pi^0}}. \tag{3.11}$$

Further constrain was applied on π^0 mass, in order to keep the π^0 mass at the constrained mass. We modified the momentum of π^0 using factor

$$\alpha = \sqrt{(1-(1-s^2)\frac{E^2_{\pi^0}}{P^2_{\pi^0}})}. \tag{3.12}$$

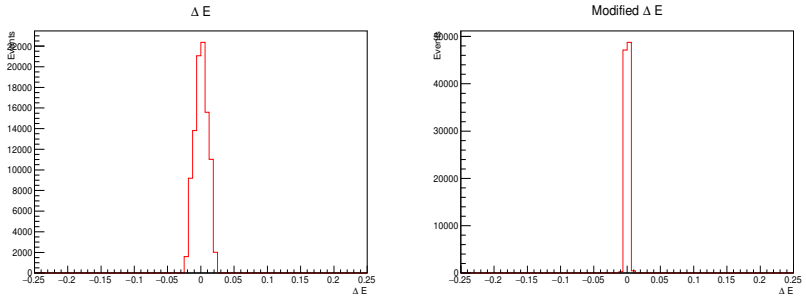

Figure 3.14: unmodified ΔE(left) and modified ΔE(right) from signal MC.

In Fig 3.15 plot of modified $M_{J/\psi\omega}$ and modified $M_{K\omega}$ are shown. We can clearly see that, even after modification of π^0 momentum $M_{K\omega} > 1.4$ GeV/c^2 can be applied.

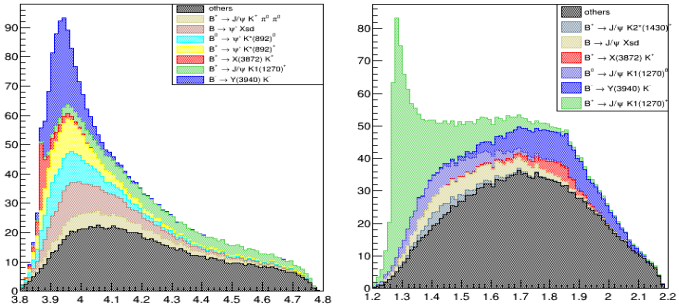

Figure 3.15: modified $M_{J/\psi\omega}$(left) and modified $M_{K\omega}$(right) from Inclusive MC.

3.8 Background suppression

3.8.1 $\psi' K^*$ Veto

We got the background $B \to \psi' K^*$ decay mode in reconstructed events. We applied $\psi' K^*$ veto in order to remove this background. We expects $J/\psi\pi^+\pi^-$ from ψ' decay and $K\pi^0$ from K^* decay. 1D-plot of invariant mass of $J/\psi\pi^+\pi^-$ and $K\pi^0$ shown in Fig 3.16. 2D-plot of mass of $J/\psi\pi^+\pi^-$ and $K\pi^0$ shown in, Fig 3.16. We are rejecting the following region: 3.67 GeV/c^2 $< M_{J/\psi\pi^+\pi^-} <$ 3.72 GeV/c^2 and 0.79 GeV/c^2 $< M_{K\pi^0} <$ 0.99 GeV/c^2 in order to reject $B \to \psi' K^*$ events.

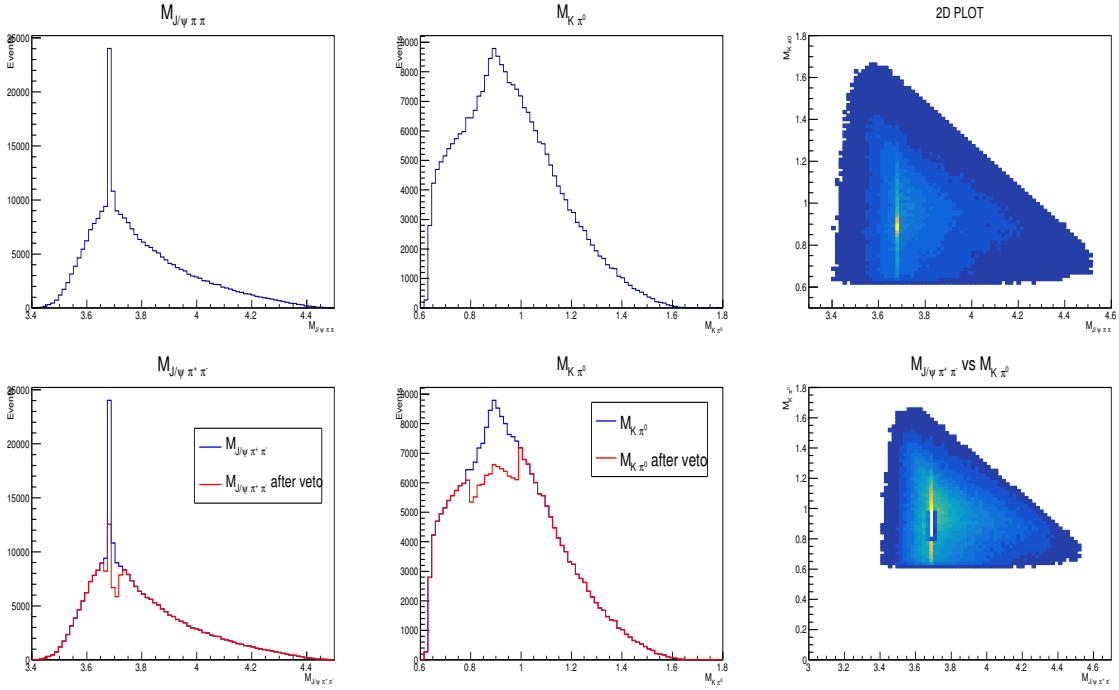

Figure 3.16: (Above) plot of $M_{J/\psi\pi^+\pi^-}$ (left) and $M_{K\pi^0}$ (centre) and 2-D plot of $M_{J/\psi\pi^+\pi^-}$ and $M_{K\pi^0}$ (right) from inclusive MC. (Below) overlapped histogram of $M_{J/\psi\pi^+\pi^-}$ with $M_{J/\psi\pi^+\pi^-}$ veto (left), $M_{K\pi^0}$ with $M_{K\pi^0}$ veto (centre) and 2-D plot of $M_{J/\psi\pi^+\pi^-}$ and $M_{K\pi^0}$ with veto (right) from inclusive MC.

3.9 Comparison

3.9.1 Background Comparison

Comparison of the $M_{J/\psi\omega}$ is done in Fig 3.17. As seen there is improvement in resolution.

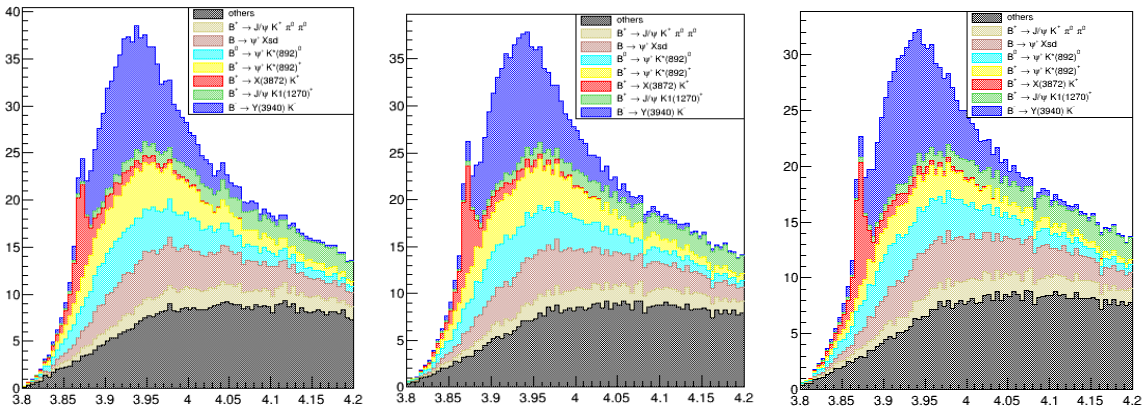

Figure 3.17: Plot of $M_{J/\psi\omega}$ from Inclusive MC. Unmodified $M_{J/\psi\omega}$ (left), modified $M_{J/\psi\omega}$ (centre) and modified $M_{J/\psi\omega}$ with veto (right).

3.9.2 Signal Comparison

Overlapping the unmodified $M_{J/\psi\omega}$, and modified $M_{J/\psi\omega}$ from signal MC we can see that there is improvement in signal resolution, Fig 3.18.

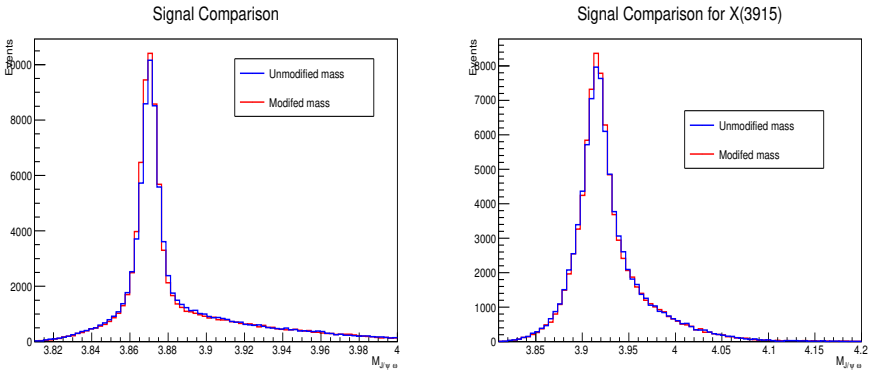

Figure 3.18: $M_{J/\psi\omega}$ for $B^{\pm} \to X(3872)K^{\pm}$ events (left) and $M_{J/\psi\omega}$ for $B^{\pm} \to X(3915)K^{\pm}$ events (right) from signal MC.

3.10 Signal Efficiency

Table 3.2 summarizes the final signal efficiency from signal MC. Efficiency of reconstructed events = (Number of reconstructed events in signal region applying all cuts)/(Total number of generated events).

Efficiency of the generated samples	
Signal	Efficiency(%)
$B^{\pm} \to X(3872)K^{\pm}$	9.01±0.1
$B^{0} \to X(3872)K^{0}_{S}$	5.61±0.1
$B^{\pm} \to X(3915)K^{\pm}$	8.62±0.1
$B^{0} \to X(3915)K^{0}_{S}$	5.13±0.1

Table 3.2: Final signal efficiency after applying all cut

3.11 Signal Extraction

After the study of the background and signal MC samples, we plan to extract the signal from the fit to the $M_{J/\psi\omega}$ distribution. 1DUML fit has performed for this purpose.

Sum of two Gaussians and one bifurcated Gaussian is used for signal parameterization, as shown in Fig 3.19.

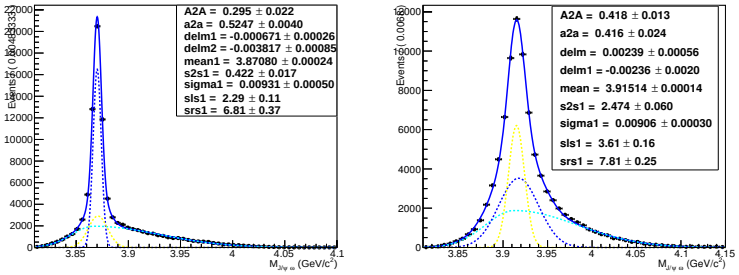

Figure 3.19: 1DUML fit to $M_{J/\psi\omega}$ distribution for $B^{\pm} \to X(3872)K^{\pm}$ (left) and $B^{\pm} \to X(3915)K^{\pm}$ (right) from signal MC.

3.11.1 Background

Backgrounds can be divided into two parts: peaking and non peaking. For background we used J/ψ inclusive MC samples($\times$100 data).

Peaking Background

Peaking background is due to $B^{+} \to \psi' K^{*}(892)^{+}$ and $B^{0} \to \psi' K^{*}(892)^{0}$ in $M_{J/\psi\omega}$ distribution. For both cases we have used one Gaussian and two bifurcated Gaussian for fit as shown in Fig 3.20.

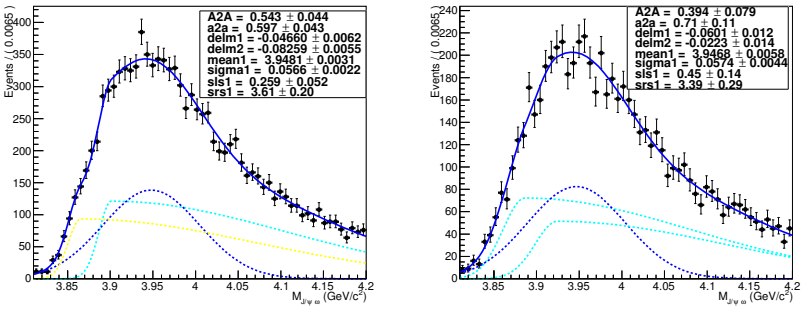

Figure 3.20: 1DUML fit to $M_{J/\psi\omega}$ distribution for $B^{+} \to \psi' K^{*}(892)^{+}$(left) and for $B^{0} \to \psi' K^{*}(892)^{0}$(right) from Signal MC.

Non peaking Background

This background is flat in the $M_{J/\omega}$ distribution. For nonpeaking background fitting from J/ψ inclusive MC samples, we have removed signal part as well as peaking backgrounds from inclusive MC samples. We used a threshold function to obtain the fit, Fig 3.21. Where threshold function is defined as,

$$(M - M_{Th})^2 \exp(a(M - M_{Th}) + b(M - M_{Th})^2 + c(M - M_{th})^3) \tag{3.13}$$

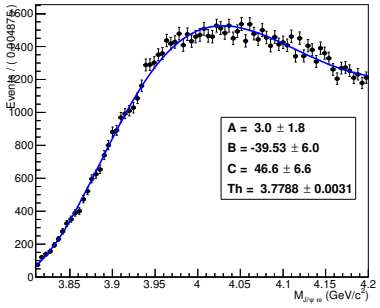

Figure 3.21: 1DUML fit to $M_{J/\psi\omega}$ distribution for non peaking backgrounds in $B^{\pm} \to X(3872)K^{\pm}$ decay mode from J/ψ Inclusive MC.

Total Background fit

Fig 3.22 describes the total background fit for $M_{J/\psi\omega}$. For total background fit from J/ψ inclusive MC samples, we have removed signal part from inclusive MC samples and only peaking and non peaking backgrounds are fitted. In fitting only fraction between flat and total peaking background has been floated.

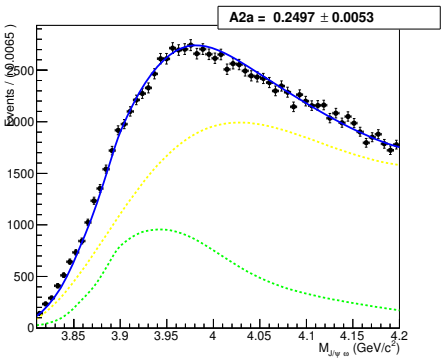

Figure 3.22: 1DUML fit to $M_{J/\psi\omega}$ distribution for total backgrounds in $B^{\pm} \to X(3872)K^{\pm}$ decay mode from J/ψ Inclusive MC.

Total $M_{J/\psi\omega}$ fit

Fig 3.23 describes the total $M_{J/\psi\omega}$ fit. For total $M_{J/\psi\omega}$ fit, only signal($X(3872)$ and $X(3915)$) fraction and flat background fraction has been floated.

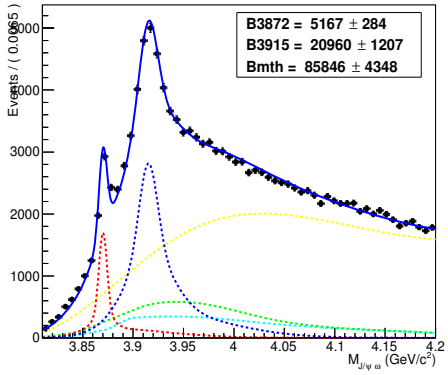

Figure 3.23: 1DUML fit to $M_{J/\psi\omega}$ distribution for signal and background in $B^{\pm} \to X(3872)K^{\pm}$ decay mode from J/ψ Inclusive MC.

3.12 Branching fraction

We determine the branching fraction, $\mathcal{B}(B \to XK) \times \mathcal{B}(X \to J/\psi\omega)$, where X may be $X(3872)$ or $X(3915)$. Using the relation

$$\mathcal{B} = \frac{N_{event}}{N_{B\bar{B}} \times \epsilon \times f_K \times \mathcal{B}_{secondary}} \tag{3.14}$$

where N_{event} is the number of events for a particular mode, $N_{B\bar{B}} = (772\pm11)\times10^6$, is the number of $N_{B\bar{B}}$ events in the data, $B_{secondary}$ is the secondary branching fractions $\mathcal{B}(J/\psi \to l^+l^-) = 0.119\pm0.001$ and $\mathcal{B}(\omega \to \pi^+\pi^-\pi^0) = 0.892\pm0.007$, $\mathcal{B}(\pi^0 \to \gamma\gamma) = 0.98\pm0.00034$, depending on the mode, ϵ is the efficiency estimated from the signal MC. f_K is the coefficient to incorporate $\mathcal{B}(K^0 \to K^0_s)$ and set to be 0.5 and 1 for neutral and charged modes, respectively.

Branching fraction of respective modes				
Decay mode	Efficiency(ϵ)(%)	N_{event}	DECAY.DEC	Measured
$B^{\pm} \to X(3872)K^{\pm}$	9±0.1	51±3	10.3×10^{-6}	$(7.02 \pm0.4) \times 10^{-6}$
$B^{\pm} \to X(3915)K^{\pm}$	8.6±0.1	209±12	7.1×10^{-5}	$(3.03 \pm0.2)\times 10^{-5}$

Table 3.3: Branching fraction for $B^{\pm} \to X(3872)K^{\pm}$ and $B^{\pm} \to X(3915)K^{\pm}$ decay mode

3.13 Toy MC Study

We have generated 2000 toy MC samples using signal and background PDFs for $M_{J/\psi\omega}$ distribution. Signal PDF is generated using 44 signal yield for $X(3872)$ (as expected using PDG B.R $(6.0 \pm 2.2) \times 10^{-6}$) and 211 (as expected using PDG B.R $(3.0^{+0.9}_{-0.7}) \times 10^{-5}$) signal yield for $X(3915)$ for $M_{J/\psi\omega}$.

We performed the unbinned likelihood fit for generated toy samples in order to extract the signal yield and estimate the bias by calculating the pull. Fig 3.24 shows the yield distribution and pull distribution for $M_{J/\psi\omega}$ which demonstrate that there is no significant bias in final fitter.

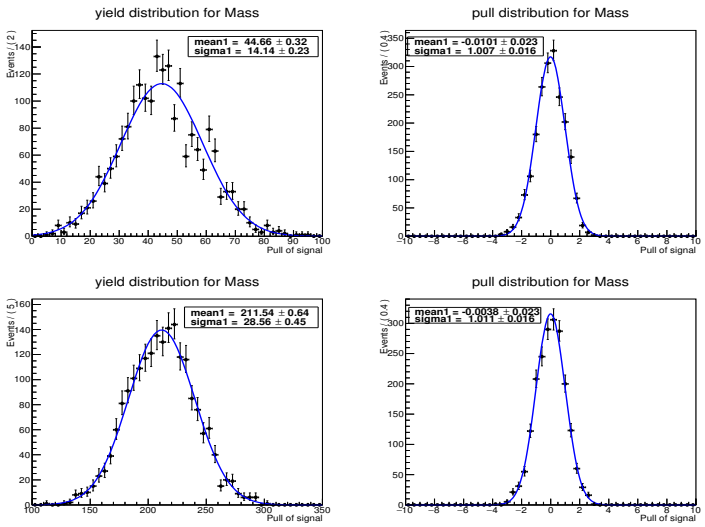

Figure 3.24: Yield and pull distribution for $B^{\pm} \to X(3872)K^{\pm}$ decay(top) and $B^{\pm} \to X(3915)K^{\pm}$ decay(bottom). Yield fixed for $X(3872)$ is 44 and for $X(3915)$ is 211.

3.13.1 Linearity Test

The linearity test of the signal yield is performed from 44 to 80 for $X(3872)$ and from 150 to 350 for $X(3915)$. For this test 2000 toys are generated at each step. Results of the linearity test of output yield and pull sigma is shown in Fig 3.25. Which shows that fitter is stable.

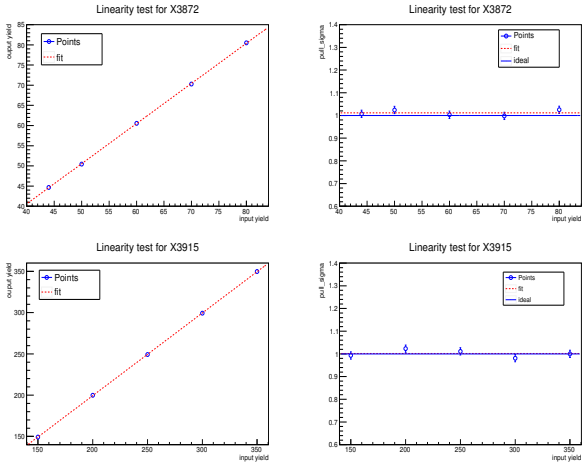

Figure 3.25: (left) Input versus output signal yield and (right) input signal yield versus pull sigma fitted with straight line (red solid line). Blue dashed line shows the behavior of pull sigma in ideal case.

3.14 GSIM Study

In GSIM test, we test the fit bias in a more realistic scenario. We divided the inclusive MC sample into 100 samples (after removing $B^{\pm} \to X(3872)K^{\pm}$ and $B^{\pm} \to X(3915)K^{\pm}$ signal part) and embed signal from signal MC with the same yield as used in toy MC. Results of GSIM yield distribution and pull distribution for $M_{J/\psi\omega}$ shown in Fig 3.26. 3.4% and 0.5 % bias is observed for $B^{\pm} \to X(3872)K^{\pm}$ and $B^{\pm} \to X(3915)K^{\pm}$ decay mode respectively and will be included in the systematics.

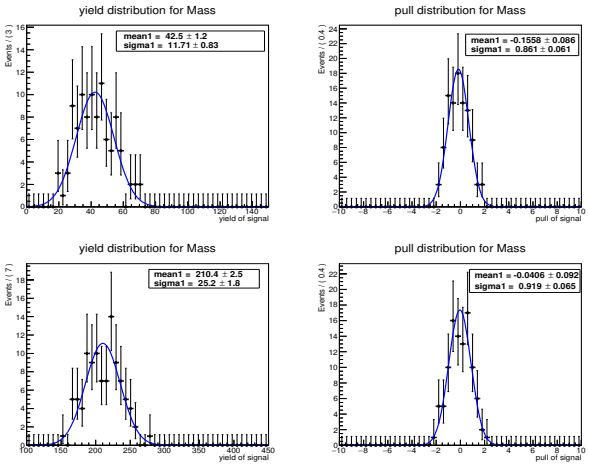

Figure 3.26: GSIM study for $X(3872)$(top), with yield 44 and $X(3915)$ (bottom), with yield 211.

3.15 M_{bc} Study

As we plan to fix the parameters of $M_{J/\psi\omega}$, we will use M_{bc} to estimate the resolution difference between data and MC.

3.15.1 Background Study

To study the possible sources of background, $B \to J/\psi X$ inclusive MC samples are analyzed (100× data). Fig 3.27 (left) shows the background distribution along with signal of beam constrained mass (M_{bc}).

3.15.2 Signal extraction

After the study of the background and signal MC samples, we plan to extract the signal from the fit to the M_{bc} distribution. 1DUML fit is performed for this purpose. We have used $B \to J/\psi\omega K$ mode i.e PHSP part as the signal. Sum of logarithmic Gaussian and Gaussian is used for signal parameterization. Fig 3.27(right) shows the fit to $B \to J/\psi\omega K$ decay mode.

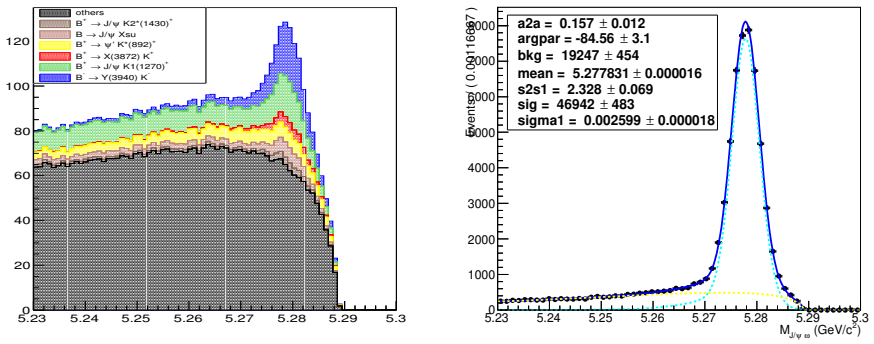

Figure 3.27: Background distribution for M_{bc} (left) from inclusive MC and 1DUML fit to M_{bc} distribution for $B \to J/\psi\omega K$ decay mode (right) from signal MC.

3.15.3 Background parameterization

Backgrounds are divided into two parts: peaking and non peaking.

Peaking background

In $M_{\rm bc}$ distribution, one gets peaking background from the $B^+ \to \psi' K^*(892)^+$ decay mode. This is due to the same event topology $B^+ \to \psi'(\to J/\psi\pi^+\pi^-)K^{*+}(\to K^+\pi^0)$. In order to parameterize this background, we used two bifurcated Gaussian and one Argus function to obtain the fit, Fig 3.28.

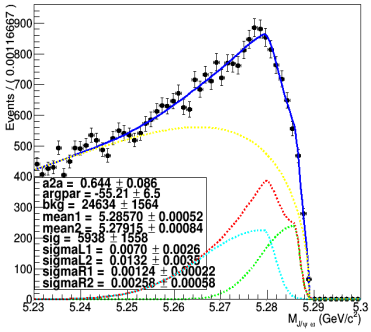

Figure 3.28: 1DUML fit to M_{bc} distribution for $B^+ \to \psi' K^*(892)^+$ decay mode from inclusive MC.

Non peaking background

Non-peaking background due to the combinatorial background in M_{bc} distribution can be parameterized by the Argus function to obtain the fit, Fig 3.29.

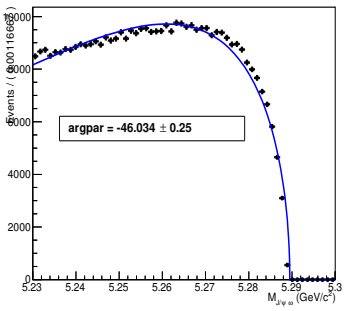

Figure 3.29: 1DUML fit to M_{bc} distribution for non peaking backgrounds in J/ψ inclusive MC.

Total M_{bc} fit

Fig 3.30 shows the total fit which includes signal and backgrounds for the M_{bc} distribution.

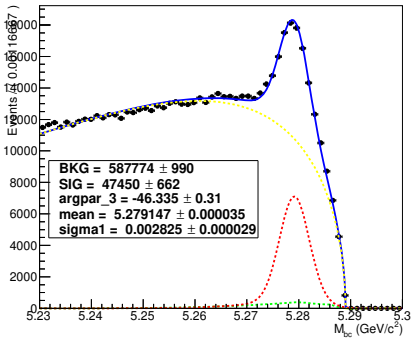

Figure 3.30: 1DUML fit to M_{bc} distribution for signal and backgrounds from inclusive MC.

3.16 Toy study

We have generated 2000 Toy MC samples using signal and background PDFs for M_{bc} distribution. Signal PDF is generated using 1231 signal yield for $B \to J/\psi\omega K$ [as expected using PDG B.R $(3.20^{+0.6}_{-0.32}) \times 10^{-4}$].

We performed the unbinned likelihood fit for generated toy samples to extract the signal yield and estimate the bias by calculating the pull. Fig 3.31 shows the yield distribution and pull distribution for M_{bc} which demonstrate that there is no significant bias in final fitter.

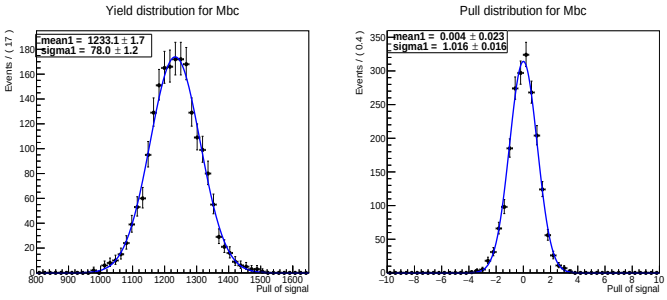

Figure 3.31: Toy study for M_{bc}.

3.16.1 Linearity test

The linearity test of the signal yield is performed from 1150 to 1350, in the interval of 50. For this test 2000 toys are generated at each step. Results of linearity test of output yield and pull sigma is shown in Fig 3.32. Which shows that fitter is stable.

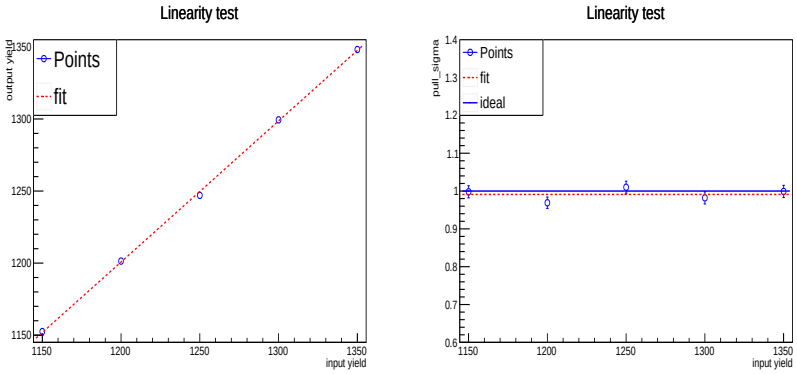

Figure 3.32: Results of linearity test for Signal Extraction of M_{bc}: (left) Input versus output signal yield and (right) Input signal yield versus pull sigma fitted with straight line (red solid line). Blue dashed line shows the behavior of pull sigma in ideal case.

3.17 Comparison of experiment no vs. luminosity in data

We have processed the data but still, have not looked at the signal region. We count the total number of events (which include signal and the background) and divided them with the luminosity in that experiment. It's done to check that we have not left any signal experiment. Fig. 3.33 shows the plot for each experiment.

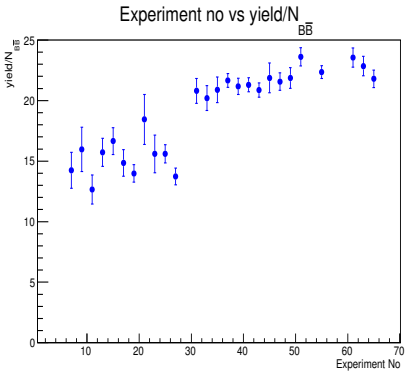

Figure 3.33: Comparison of experiment no vs yield/$N_{B\bar{B}}$.

Chapter 4

Summary & Conclusions

4.1 Concluding Remarks

$B \to (J/\psi\omega)K$ decay mode will help us to understand the nature of the $X(3872)$. In this thesis, we plan measure the ratio, $\mathcal{B}(X(3872) \to J/\psi\omega)/\mathcal{B}(X(3872) \to J/\psi\pi\pi)$. We reconstruct B meson from its final daughter particles (e^+, e^-, μ^+, μ^-, π^+, π^-, γ and K^+). We prepared the reconstruction code to analyze the $B \to (J/\psi\omega)K$ decay mode. As we found large fake B candidates due to the wrongly reconstructed ω candidates, we selected ω candidates based on its Dalitz distributions. This was found to be the best way to select the correctly reconstructed ω candidates. Using this optimized ω selection, we were able to reject 29 % of the fake events. After full reconstruction, one expects only one B candidate per event. However, we found that still after reconstructing B meson, out of total events 35% events still have multiple B candidates. To select the best candidates from the multiple B candidates, we compared two methods: a) minimum of χ^2 method [sum of charged track vertex fitting χ^2 and invariant mass χ^2] and b) M_{bc} closest to the nominal B mass. We found the χ^2 method to be the best. In the minimum of χ^2 method, we were able to reject 83 % of the total fake candidates.

We further identify the backgrounds sources for our study. Potential backgrounds were identified using $B \to J/\psi X$ inclusive MC samples. We applied $M_{K\omega} > 1.4$ GeV/c^2 cut to reject the contributions coming from the higher K^* resonances. Although, after

applying all cuts and selection criterion's, poor resolution in the signal was still seen. Background coming from $B \to \psi' K^*$ was removed after using $\psi' K^*$ veto. An attempt to improve the resolution was made by applying π^0 momentum modification, which result in a small improvement in the resolution of signal and background events.

After applying all cut's and criterion's we estimated the reconstruction efficiency for $B \to X(3872)\ K$ decay mode to be is about (9.0±0.1)% and for $B \to X(3915)\ K$ is about (8.6±0.1)%. 1D unbinned maximum likelihood fit is done on $B \to J/\psi X$ inclusive MC samples to extract the signal yield. From fitting we expect 51±3 and 209 ±12 events for $B \to X(3872)K$ and $B \to X(3915)K$ decay mode and the corresponding branching fraction is (7.0±0.4(stat))$\times 10^{-6}$ and (3.1±0.2(stat)) $\times 10^{-5}$, respectively. By performing fit bias studies, we concluded that fitters are stable. As we fixed the parameters of $M_{J/\psi\omega}$, we plan to use $M_{\rm bc}$ to estimate the resolution difference between data and MC. We have processed the data without looking at the signal region. We looked at the total events and divided it by the luminosity to check for any potential problem in the data processing.

4.2 Future Outlook

Final signal extraction procedure has been established. We have submitted the Belle Note (Internal Belle Note No.- 1516) to the collaboration and currently waiting for the internal referees to get their permission to open the box (look at the data). After the referee's permission, we plan to look and fit the data. We plan to perform simultaneous fits to the charged and neutral B decay modes.

Appendix - A

Appendices

1 Decay files for signal generation

$X(3872)$

Alias MyB+ B+

Alias MyB- B-

Alias MyJpsi J/psi

Alias Myomega omega

Alias MyX3872 X(3872)

Decay Upsilon(4S)

0.5 MyB+ B- VSS;

0.5 B+ MyB- VSS;

Enddecay

Decay MyB+

1.0 MyX3872 K+ PHOTOS PHSP;

Enddecay

Decay MyB-

1.0 MyX3872 K- PHOTOS PHSP;

Enddecay

Decay MyX872

1.0 MyJpsi Myomega PHOTOS PHSP;

Enddecay

Decay MyJpsi

0.0593 $e+$ $e-$ PHOTOS VLL;

0.0588 $mu+$ $mu-$ PHOTOS VLL;
Enddecay

Decay Myoemga
0.89401 pi+ pi- pi0 PHOTOS OMEGA_ DALITZ;
Enddecay End

$X(3915)$

Alias MyB+ B+
Alias MyB- B-
Alias MyJpsi J/psi
Alias Myomega omega
Alias MyX3915 X(3915)

Decay Upsilon(4S)
0.5 MyB+ B- VSS;
0.5 B+ MyB- VSS;
Enddecay

Decay MyB+
1.0 MyX3915 K+ PHOTOS PHSP;
Enddecay

Decay MyB-
1.0 MyX3915 K- PHOTOS PHSP;
Enddecay

Decay MyX3915
1.0 MyJpsi Myomega PHOTOS PHSP;
Enddecay

Decay MyJpsi
0.0593 $e+$ $e-$ PHOTOS VLL;

0.0588 $mu+$ $mu-$ PHOTOS VLL;
Enddecay

Decay Myoemga
0.89401 pi+ pi- pi0 PHOTOS OMEGA_ DALITZ;
Enddecay End

Appendix - B

2 Omega optimization table

Centre	Radius1	Radius2	Signal Rejection(in %)	Fake Rejection(in %)
(0 3)	1.5	3.9	3.7	20.2
(0 3)	1.4	3.9	3.4	19.9
(0 3)	1.5	3.8	7.3	28.5
(0 -7)	6.35	8.6	8.5	28.4
(0 -7)	6.3	8.6	6.2	23.4
(0 -7)	6.3	8.5	6.5	23.8
(0 -7)	6.4	8.5	11.3	33.3
(0 4)	2.5	4.8	6.6	27.1
(0 3.5)	2	4.3	7	27.7

Table 4.1: ω cut optimization table for $B^{\pm} \to X(3872)K^{\pm}$.

Bibliography

[1] S.-K. Choi *et al.* (Belle Collaboration), Phys. Rev. Lett. **91**, 262001 (2003).

[2] T. Aushev *et al.* (Belle Collaboration), Phys. Rev. D **81**, 031103(R) (2010).

[3] B. Aubert *et al.* (BABAR Collaboration), Phys. Rev. Lett. **102**, 132001 (2009).

[4] V. Bhardwaj *et al.* (Belle Collaboration), Phys. Rev. Lett. **107**, 091803 (2011).

[5] R. Aaij *et al.* (LHCb Collaboration), Nucl. Phys. B **886**, 665 (2014).

[6] P. del Amo Sanchez *et al.* (BABAR Collaboration), Phys. Rev. D **82**, 011101(R) (2010).

[7] R. Mitchell *et al.* (BESIII Collaboration), "Experimental Aspects of Heavy Quark Exotica: A Brief Tour of the XYZ", XIII $^{\text{th}}$ Quark Confinement and the Hadron Spectrum, Ireland (August 2, 2018).[https://indico.cern.ch/event/648004/contributions/3027579/attachments/1696395/2730648/MitchellXYZ.pdf]

[8] T. Iwashita *et al.* (Belle Collaboration), Progress of Theoretical and Experimental Physics, 043C01 (2014).

[9] The BELLE collaboration, Vinokurova, A., Kuzmin, A. *et al.*, J. High Energ. Phys. (2015) 2015: 132. https://doi.org/10.1007/JHEP06(2015)132.

[10] S. K. Choi. arXiv:1101.5691 (2011).

[11] Kunihiko Terasaki, arXiv:1411.7483 (2014).

[12] K. Abe, *et al.* (Belle Collaboration), arXiv:hep-ex/0505037 (2005).

[13] P. del Amo Sanchez *et al.* (BABAR Collaboration), Phys. Rev. D **82**, 011101(R) (2010).

[14] arXiv:1903.04695 [hep-ex].

[15] D.J. Lange, Nucl. Instrum. Methods Phys. Res. A 462,152 (2001).

[16] Charge-conjugate modes are included throughout the analysis unless stated otherwise.

[17] R. Brun *et al.,* GEANT3.21, CERN Report No. DD/EE/84-1, 1984.

[18] Charmonium Group "Event Selection of $B \to J/\psi K_S$", Internal Belle Note 318.

[19] G. Fox and S. Wolfram, Phys. Rev. Lett. **41**, 1581 (1978).